

DSTED: Decoupling Temporal Stabilization and Discriminative Enhancement for Surgical Workflow Recognition

Yueyao Chen¹, Kai-Ni Wang¹, Dario Tayupo², Arnaud Huaulmé²,
Krystel Nyangoh Timoh², Pierre Jannin², Qi Dou^{1*}

¹Department of Computer Science and Engineering, The Chinese University of Hong Kong, Hong Kong, China.

²Univ Rennes, Inserm, LTSI - UMR 1099, 35000, Rennes, France.

*Corresponding author(s). E-mail(s): qidou@cuhk.edu.hk;

Contributing authors: yychen@cse.cuhk.edu.hk;

kainiwang@cuhk.edu.hk; dario.tayupo@univ-rennes.fr;

arnaud.huaulme@univ-rennes.fr; krystel.nyangoh.timoh@chu-rennes.fr;

pierre.jannin@univ-rennes.fr;

Abstract

Purpose: Surgical workflow recognition enables context-aware assistance and skill assessment in computer-assisted interventions. Despite recent advances, current methods suffer from two critical challenges: prediction jitter across consecutive frames and poor discrimination of ambiguous phases. This paper aims to develop a stable framework by selectively propagating reliable historical information and explicitly modeling uncertainty for hard sample enhancement.

Methods: We propose a dual-pathway framework DSTED with Reliable Memory Propagation (RMP) and Uncertainty-Aware Prototype Retrieval (UPR). RMP maintains temporal coherence by filtering and fusing high-confidence historical features through multi-criteria reliability assessment. UPR constructs learnable class-specific prototypes from high-uncertainty samples and performs adaptive prototype matching to refine ambiguous frame representations. Finally, a confidence-driven gate dynamically balances both pathways based on prediction certainty.

Results: Our method achieves state-of-the-art performance on AutoLaparohysterectomy with 84.36% accuracy and 65.51% F1-score, surpassing the second-best method by 3.51% and 4.88% respectively. Ablations reveal complementary

gains from RMP (2.19%) and UPR (1.93%), with synergistic effects when combined. Extensive analysis confirms substantial reduction in temporal jitter and marked improvement on challenging phase transitions.

Conclusion: Our dual-pathway design introduces a novel paradigm for stable workflow recognition, demonstrating that decoupling the modeling of temporal consistency and phase ambiguity yields superior performance and clinical applicability.

Keywords: Surgical workflow recognition, Dual-pathway learning, Temporal modeling, Memory propagation

1 Introduction

Surgical workflow recognition enables understanding of surgical procedures by automatically identifying operative phases. Accurate phase recognition is crucial for context-aware assistance and objective skill assessment [1]. In clinical practice, reliable workflow understanding can facilitate intraoperative decision support [2], and streamline surgical training, making it a key capability for intelligent operating rooms.

While recent deep learning methods have achieved notable progress, two fundamental challenges remain unresolved: **temporal instability** [3] and **poor generalization to ambiguous phases** [4]. Temporal instability manifests as prediction jitter across consecutive frames (Fig. 1 (a)), where phase classifications fluctuate erratically despite minimal visual changes. Poor generalization to ambiguous phases leads to inadequate discrimination of challenging frames and underrepresented classes (Fig. 1 (b)), compromising overall recognition robustness. These issues are particularly pronounced in complex surgery with severe phase imbalance, high inter-phase similarity, and gradual temporal transitions.

Recent advances in temporal modeling have significantly improved sequence understanding. Early CNN-LSTM architectures [5] established a foundation for temporal reasoning, which was later refined by multi-stage temporal networks [6], and Transformer-based designs [7] that exploit long-range dependencies through self-attention. More recently, state space models [8] offer efficient multi-scale temporal context modeling. However, existing approaches largely adopt a unified temporal reasoning framework, processing all frames indiscriminately, and coupling temporal modeling with feature discrimination in a single stream.

We posit that temporal instability and hard-sample misclassification constitute two modes that require specialized treatment. A unified model inherently faces conflicting optimization objectives, as temporal smoothness requires consistency across frames to suppress jitter, while discriminative separation demands class-separable boundaries to distinguish ambiguous phases. Enforcing one often compromises the other. Temporal jitter arises not from insufficient context, but from indiscriminate propagation of unreliable predictions during ambiguous transitions, as models lack confidence-aware filtering mechanisms. Conversely, poor recognition of rare or ambiguous phases stems

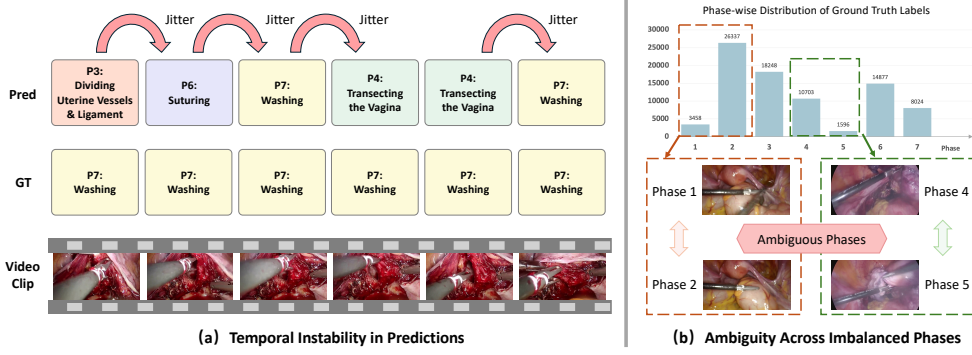


Fig. 1 (a) Prediction jitter across adjacent frames, where phase classifications fluctuate significantly despite minimal visual changes. (b) Ambiguous phase predictions caused by class imbalance and high inter-phase similarity, leading to confusion between visually overlapping surgical stages.

not merely from data imbalance, but from insufficient uncertainty modeling to capture discriminative patterns in challenging samples. This motivates our central insight that temporal stabilization and discriminative enhancement should be decoupled yet complementary objectives.

To this end, we propose **DSTED**, a dual-pathway framework that decouples the stabilization–temporal and enhancement–discriminative pathways for surgical workflow recognition. The first pathway, Reliable Memory Propagation (**RMP**), stabilizes frame-wise predictions by maintaining a dynamic memory of historical features and selectively propagating only those with high reliability. Reliability is jointly assessed through feature similarity, class consistency, and temporal proximity, ensuring that only temporally coherent context contributes to the current representation while suppressing unstable information. The second pathway, Uncertainty-Aware Prototype Retrieval (**UPR**), targets ambiguous or hard-to-distinguish frames by leveraging class-specific prototypes derived from high-uncertainty training samples. During inference, it refines representations via similarity-based prototype retrieval, enhancing discrimination under uncertainty. Finally, a confidence-driven gating mechanism dynamically integrates both pathways, adaptively balancing temporal guidance and prototype refinement based on prediction certainty to achieve stable predictions. In summary, our main contributions are as follows:

1. We introduce a novel dual-pathway architecture that decouples temporal stabilization from discriminative enhancement, addressing two fundamental failure modes in surgical workflow recognition.
2. We design reliable memory propagation with multi-criteria reliability assessment for selective temporal consistency and uncertainty-aware prototype retrieval with class-specific uncertainty modeling for robust recognition of ambiguous phases.
3. We achieve state-of-the-art performance on the AutoLaparo dataset [9] with extensive ablations confirming the complementary contributions of both pathways, their synergistic effects, and substantial improvements in both accuracy and temporal stability.

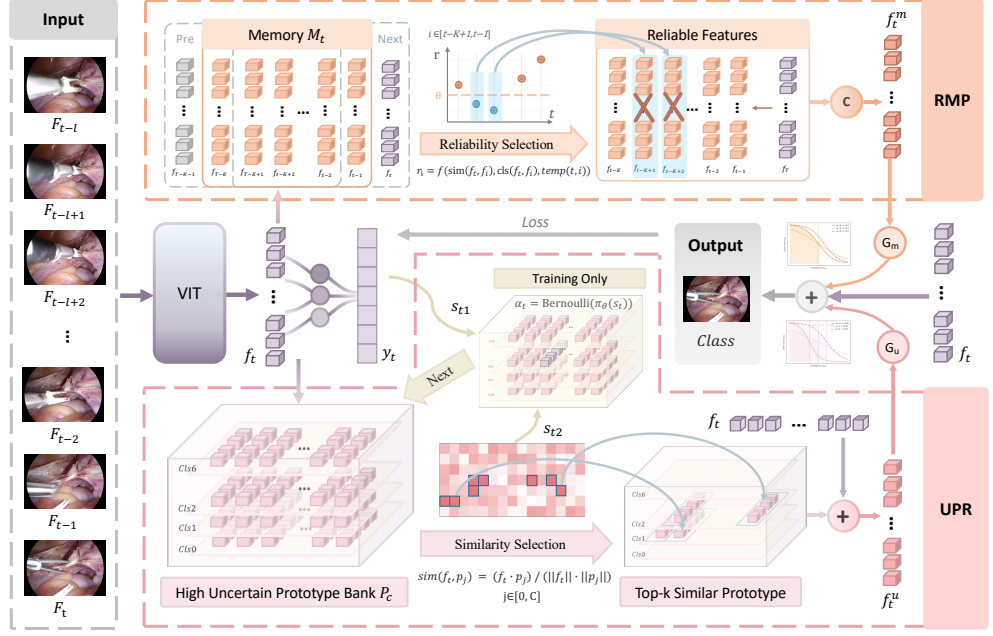


Fig. 2 Overview of the proposed framework with reliable memory propagation and uncertainty-aware prototype retrieval, integrated via confidence-driven gating.

2 Method

The framework consists of three core components (Fig. 2). Section 2.2 presents reliable memory propagation, which maintains a dynamic memory bank and employs multi-criteria reliability assessment to filter and propagate temporal context. Section 2.3 describes the uncertainty-aware prototype retrieval, which constructs class-specific prototypes from high-uncertainty samples and performs similarity-based retrieval during inference. Section 3.4 introduces the confidence-driven integration mechanism and the training objective.

2.1 Overview

Given a surgical video V with T frames, we extract spatiotemporal features using a Vision Transformer (ViT) that processes temporal clips of length l : $f_t = \text{ViT}(I_t)$, $f_t \in \mathbb{R}^D$, where $I_t = \{I_{t-l+1}, \dots, I_t\}$ denotes the clip in timestep t , and D is the dimension of the feature. A causal temporal head produces baseline logits and predictions:

$$y_t^{base} = W_{cls} \cdot f_t, p_t^{base} = \text{softmax}(y_t^{base}) \quad (1)$$

where $W_{cls} \in \mathbb{R}^{C \times D}$ and C is the number of surgical phases. To enhance temporal stability, RMP computes a refined feature f_t^m by selectively aggregating reliable memories from a sliding window: $f_t^m = \text{RMP}(f_t, M_t)$, where $M_t = \{f_{t-K}, \dots, f_{t-1}\}$ represents

the memory bank containing features of the most recent K timesteps. Simultaneously, UPR refines the representation by retrieving relevant prototypes from class-specific banks: $f_t^u = UPR(f_t, P)$, where $P = \{P_1, \dots, P_C\}$ denotes the collection of prototype banks for all classes. A confidence-driven gating mechanism adaptively integrates the three features based on baseline confidence.

$$f_{final} = f_t + g_m \cdot f_t^m + g_u \cdot f_t^u \quad (2)$$

where g_m and g_u are gate weights computed from p_t^{base} . This architecture enables dynamic balancing between temporal stability from RMP and discriminative enhancement from UPR.

2.2 Reliable Memory Propagation

Reliable memory propagation is designed to stabilize temporal predictions by selectively leveraging historical context. RMP addresses the challenge that not all historical frames are equally reliable, and blindly incorporating low-confidence predictions from ambiguous transitions can amplify temporal jitter. To overcome this, RMP maintains a dynamic memory bank of recent features and employs multi-criteria reliability assessment to filter and propagate only high-confidence temporal information.

Memory Bank Design. At each timestep t , RMP maintains a first-in-first-out memory bank $M_t = \{f_{t-K}, \dots, f_{t-1}\}$ containing features from the most recent K timesteps. As new features are extracted, the oldest entry is removed to maintain a fixed memory size. This sliding window design ensures that RMP focuses on recent temporal context relevant to the current frame while avoiding computational overhead from storing the entire video history.

Multi-Criteria Reliability Assessment. To determine which historical features are reliable for propagation, RMP evaluates each memory entry $f_i \in M_t$ through three complementary criteria. (1) Feature similarity measures the semantic alignment between the current feature f_t and historical feature f_i as $s_{sim}(f_t, f_i) = (f_t \cdot f_i) / (||f_t|| \cdot ||f_i||)$, where higher similarity indicates consistent visual content. (2) Class consistency evaluates the agreement between baseline predicted phase distributions. Given p_t^{base} and $p_i^{base} = softmax(y_i^{base})$, we compute $s_{cls}(f_t, f_i) = (p_t^{base})^\top \cdot p_i^{base}$, where higher consistency suggests stable phase predictions. (3) Temporal proximity penalizes distant memories through exponential decay as $s_{temp}(t, i) = \exp(-|t - i|/\tau)$, where τ controls the decay rate and nearby frames receive higher weights. The overall reliability score for each memory entry is computed as a weighted combination:

$$r_i = s_{sim}(f_t, f_i) + s_{cls}(f_t, f_i) + s_{temp}(t, i) \quad (3)$$

Selective Propagation. To retain only the most reliable memories, RMP applies threshold-based filtering: only memory entries with $r_i > \theta$ are retained for aggregation, where θ is a predefined reliability threshold. The selected memories are weighted by their normalized reliability scores $w_i = \exp(r_i) / \sum_j \exp(r_j)$, for $r_i > \theta$, where the summation is over all selected entries. The refined feature is obtained by applying a convolution to the weighted memories and the current feature: $f_t^m = \text{Conv}(f_t, \{w_i \cdot$

$f_i | r_i > \theta \}).$ This selective propagation mechanism ensures that only temporally coherent and confident historical information contributes to the current frame, effectively suppressing spurious fluctuations caused by ambiguous transitions.

2.3 Uncertainty-Aware Prototype Retrieval

While RMP stabilizes predictions across time by filtering unreliable temporal context, many recognition errors stem from the inherent difficulty of individual frames rather than temporal inconsistency. UPR addresses this orthogonal problem by explicitly capturing discriminative patterns from hard training samples. The key insight is that challenging cases, though often under-represented, contain critical boundary information that defines class separability. UPR constructs class-specific prototype banks from high-uncertainty features during training, then retrieves and leverages these learned hard-sample patterns to refine ambiguous predictions during inference.

Uncertainty Prototype Bank Construction. During training, UPR maintains a prototype bank P_c for each surgical phase $c \in \{1, \dots, C\}$, where each bank stores the N most uncertain features encountered for that class. At each training step, given a feature f_t with ground-truth label c and baseline prediction p_t^{base} , we compute the uncertainty score as: $u_t = 1 - \max(p_t^{base})$, which measures confidence inversely. To determine whether to add f_t to the prototype bank, we employ a lightweight policy network that makes a binary decision based on the current state. Specifically, we construct a state vector s_t encoding the uncertainty u_t , prediction entropy, confidence margin, and current bank occupancy. The policy network π_θ outputs a probability distribution over actions $\{add, skip\}$, and we sample an action:

$$a_t \sim \text{Bernoulli}(\pi_\theta(s_t)) \quad (4)$$

If $a_t = add$ and the prototype bank P_c has not reached capacity N , the feature f_t is inserted. When the bank is full, we compare u_t with the uncertainty scores of existing prototypes and replace the least uncertain entry if u_t is higher. This policy-guided collection strategy ensures that each prototype bank captures the most challenging and discriminative patterns for its corresponding phase.

Prototype Retrieval. During inference, given a current feature f_t with baseline prediction p_t^{base} , UPR retrieves relevant prototypes to refine the representation. We first compute the similarity between f_t and all prototypes across classes $\text{sim}(f_t, p_j) = (f_t \cdot p_j) / (\|f_t\| \cdot \|p_j\|)$, where p_j denotes a prototype from any class-specific bank. To focus retrieval on the most relevant classes, we weight each prototype by its class probability: $s_j = p_t^{base}[c_j] \cdot \text{sim}(f_t, p_j)$, where c_j is the class label of prototype p_j . We then select the top- k prototypes with the highest weighted similarity scores. The refined feature is obtained by aggregating the selected prototypes with similarity-based weights:

$$f_t^u = f_t + \sum_{j \in \text{top-}k} w_j \cdot p_j \quad (5)$$

where $w_j = \text{softmax}(\text{sim}(f_t, p_j))$ normalizes the similarity scores across selected prototypes. This prototype-based refinement enhances the discriminative power of

Table 1 Quantitative comparison with state-of-the-art methods on the AutoLaparo dataset.

Method	Accuracy	Jaccard	Precision	Recall	F1
ResNet	68.99	36.97	51.52	49.89	47.46
SV-RCNet	75.88	44.54	59.23	56.66	54.67
TeCNO	76.25	44.87	58.06	56.41	54.48
OHFM	76.61	45.08	58.40	56.36	54.52
TMRNet	79.49	50.13	61.89	61.36	58.52
VideoMAE-V2	79.61	48.85	63.33	58.42	57.41
AI-ENDO	80.85	52.42	64.01	62.48	60.63
DSTED (ours)	84.36	57.60	67.05	67.59	65.51

ambiguous frames by leveraging learned patterns from previously encountered hard samples.

2.4 Confidence-Driven Integration

To dynamically balance the contributions of RMP and UPR, we employ confidence-driven gating based on the baseline prediction confidence: $c_t = \max(p_t^{\text{base}})$. Two gate weights are computed as: $g_m = \sigma(a_m \cdot (\tau_m - c_t))$, $g_u = \sigma(a_u \cdot (\tau_u - c_t))$, where σ is the sigmoid function, τ_m , τ_u are threshold parameter, and the coefficients a_m and a_u are learnable parameters that modulate the gating sensitivity. When c_t is low, both gates increase to leverage temporal and prototype guidance; when c_t is high, the gates attenuate to preserve the original prediction. The final phase prediction is obtained as $y_t = \text{softmax}(W_{\text{cls}} \cdot f_{\text{final}})$. The overall training objective combines a class-balanced cross-entropy loss L_{CE} to address phase imbalance and a temporal smoothness regularization L_{KL} that penalizes abrupt changes between adjacent frames, formulated as $L = L_{\text{CE}} + L_{\text{KL}}$.

3 Experiments and Results

3.1 Experimental Setup

Dataset. We evaluate our method on the public AutoLaparo dataset, which comprises 21 full-length laparoscopic hysterectomy procedures with 83,243 annotated frames across seven surgical phases: Preparation, Dividing Ligament and Peritoneum, Dividing Vessels, Transecting the Vagina, Specimen Removal, Suturing, and Washing. The dataset exhibits substantial challenges, including significant phase imbalance, high intra- and inter-case variability, and gradual phase transitions. We perform three-fold cross-validation with 14 training and 7 testing cases per fold, reporting averaged performance across all folds.

Implementation details. We utilize VideoMAE-V2 as the backbone, with temporal clip length $l = 16$. Training is conducted using the AdamW optimizer with an initial learning rate of 1×10^{-3} and cosine annealing over 50 epochs. For RMP, we set the memory bank size to $K = 60$ (corresponding to one minute of surgical video) and

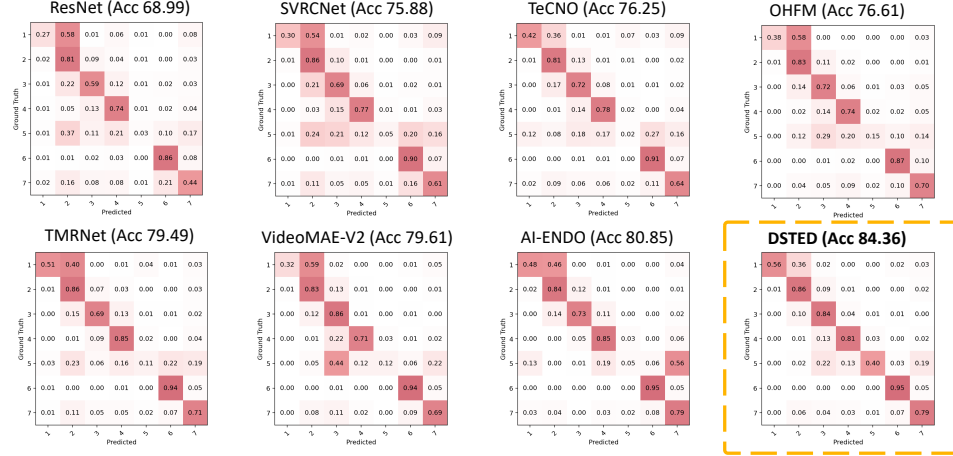


Fig. 3 Confusion matrices on the AutoLaparo dataset comparing TGMA with all baseline methods.

reliability threshold $\theta = 0.75$. For UPR, we maintain $N = 256$ prototypes per class and retrieve the top- $k = 8$ most similar prototypes during inference. All experiments are performed on a single NVIDIA A100 GPU with batch size 12.

Evaluation metrics. We report frame-level accuracy, Jaccard index, precision, recall, and F1 score to comprehensively assess classification correctness, temporal overlap quality, and robustness to class imbalance. Additionally, we provide confusion matrices to visualize inter-phase misclassifications and temporal consistency, offering further insight into the model’s discriminative and temporal reasoning capabilities.

3.2 Comparison with SOTA Methods

Comparative experiments are conducted against existing methods for surgical phase recognition, including approaches targeting temporal modeling and ambiguous frame recognition, each incorporating specialized designs to address these challenges. To ensure fair comparison, all models are trained and evaluated under identical settings. Quantitative results are presented in Table 1.

The proposed DSTED framework delivers the best overall results across all evaluation metrics, attaining 84.36% in accuracy, 65.51% in F1-score, and 57.60% in Jaccard index. It surpasses the second-best method AI-Endo [3] by a substantial margin of 3.51% in accuracy and 4.88% in F1-score. Among CNN-based methods, ResNet [10], serving as the spatial feature extraction baseline, records 68.99% accuracy. With temporal extensions, SV-RCNet [5] and TeCNO [6] boost accuracy to 75.88% and 76.25%, yielding clear improvements over the single-frame baseline. Incorporating memory-based temporal reasoning, TMRNet [11] further elevates accuracy to 79.49%. By introducing attention-driven temporal fusion, AI-Endo attains 80.85% accuracy and 60.63% F1. Meanwhile, OHFM [4], tailored for ambiguous frame enhancement, modestly refines phase discrimination, achieving 76.61% accuracy. The transformer-based VideoMAE-V2 [7] reaches 79.61% accuracy and 52.42% Jaccard, reflecting its strong capability in modeling spatiotemporal context. Building on this backbone, our DSTED

Table 2 The ablation studies validate the effectiveness of each proposed modules in DSTED.

Method	RMP	UPR	Integration	Accuracy	Jaccard	Precision	Recall	F1
Baseline	–	–	–	79.61	48.85	63.33	58.42	57.41
+RMP	✓	–	–	81.80	51.83	65.04	61.79	60.21
+UPR	–	✓	–	81.54	52.51	65.66	62.73	61.31
+Both	✓	✓	–	83.27	55.13	65.72	65.86	63.80
DSTED	✓	✓	✓	84.36	57.60	67.05	67.59	65.51

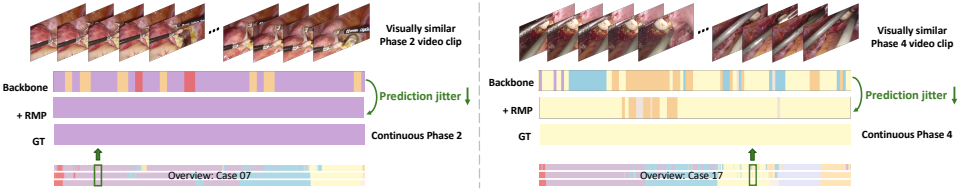


Fig. 4 Visualization of temporal prediction continuity, comparing the baseline and the model with the proposed RMP module across consecutive frames.

framework integrates RMP and UPR, leading to relative gains of 4.75% in accuracy, 5.18% in Jaccard, and 4.88% in recall.

The confusion matrices in Fig. 3 further illustrate the enhanced phase recognition capability of the proposed DSTED framework. Compared with VideoMAE-V2 and other baselines, DSTED exhibits a more pronounced diagonal distribution, reflecting reduced inter-phase confusion and more accurate classification boundaries.

3.3 Ablation Study

Ablation studies are conducted to systematically evaluate the contribution of each component (Table 2). We begin with the VideoMAE-V2 baseline and progressively incorporate individual modules: first RMP alone, then UPR alone, followed by their combination, and finally the complete framework with confidence-driven gating.

Compared with the baseline, yields a 4.75% increase in accuracy, underscoring the advantage of the combined components in improving overall recognition capability. The backbone model initially records an accuracy of 79.61%. Introducing RMP leads to a 2.19% accuracy gain over the baseline, together with rises of 3.37% in recall and 2.80% in F1-score. These results highlight the value of reliability-guided temporal memory propagation in producing more accurate and reliable phase recognition. In parallel, adding UPR reveals clear advantages of prototype-based retrieval, outperforming the baseline with a 3.66% rise in Jaccard, alongside gains of 2.51% in precision and 4.94% in recall. These improvements demonstrate the capacity of the uncertainty prototype retrieval mechanism to better distinguish challenging frames. Combining RMP and UPR provides additional benefits, as both components complement each other to deliver more accurate and discriminative predictions, yielding a 1.47% accuracy increase over RMP alone and 2.62% in Jaccard and 3.13% in recall.

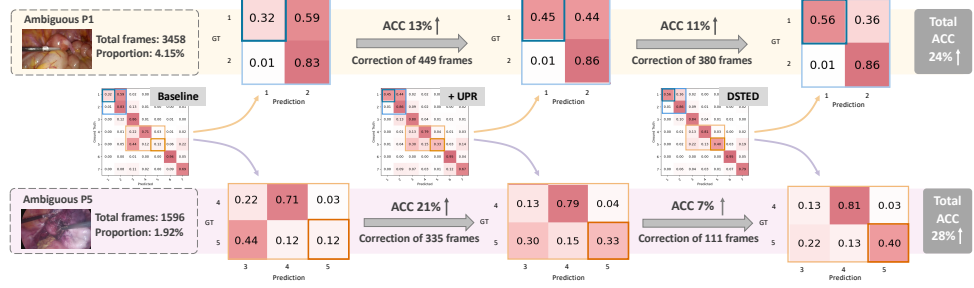


Fig. 5 Visualization of prediction improvements on ambiguous phases, illustrating the performance of the baseline, the model with UPR only, and the complete DSTED framework.

compared with UPR, respectively. With the confidence-guided integration applied, the model attains the highest overall performance, exceeding the configuration without the integration gate by 1.09% in accuracy, 2.47% in Jaccard, and 1.73% in recall. This validates underscores the efficacy of adaptively balancing memory propagation and prototype retrieval based on prediction confidence.

3.4 Effectiveness analysis

Effectiveness of temporal stability. To evaluate the impact of the short-term temporal modeling module on prediction stability, we analyze the continuity of frame-wise phase predictions. As illustrated in Fig. 4, the baseline backbone exhibits frequent fluctuations between adjacent phases within visually similar video segments, resulting in noticeable prediction jitter. With the introduction of the RMP module, such instability is substantially alleviated, producing smoother and more temporally consistent predictions that better align with the ground truth. This improvement demonstrates the designed Memory Propagation mechanism’s capability to capture short-range temporal dependencies and to propagate reliable contextual cues across neighboring frames. By enforcing temporal coherence in the feature space, the model effectively mitigates frame-level noise and suppresses spurious phase transitions, leading to more stable and reliable recognition across continuous video sequences.

Effectiveness of ambiguous frame recognition. To further assess the model’s capability in handling challenging and visually ambiguous frames, we evaluate its discrimination performance on phases with high inter-phase similarity. As shown in Fig. 5, the baseline model struggles to distinguish these visually overlapping phases, resulting in frequent misclassifications. After incorporating the UPR module, many of these confusions are progressively corrected, yielding clearer phase separation. When the complete DSTED framework is employed, recognition accuracy on these challenging frames improves further, confirming the model’s enhanced robustness in ambiguous situations. These results emphasize the effectiveness of the Uncertainty-aware Prototype Retrieval and the integration gating mechanism in improving ambiguous frame recognition and refining phase differentiation.

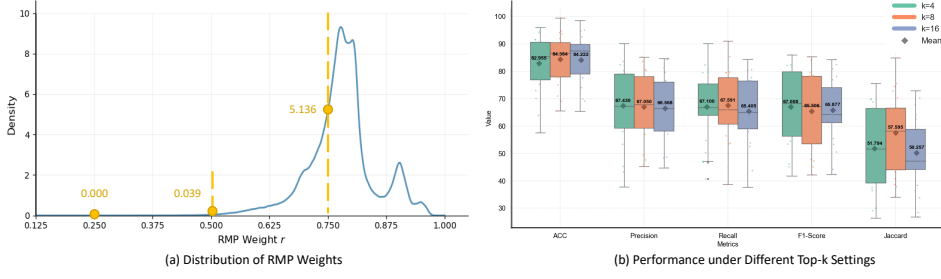


Fig. 6 (a) Distribution of reliability weights under different thresholds in RMP. (b) Performance comparison under different top- k selections in UPR.

3.5 Hyperparameter analysis

RMP Threshold. To investigate the impact of threshold θ on model performance, experiments with different threshold values were conducted, showing performance fluctuations within 1.07% (Fig. 6 (a)). The threshold determines the number of memory entries retained for propagation, where a higher threshold results in fewer memories being included. When the threshold is set to lower values (0.5 and 0.25), the filtering mechanism becomes less selective, potentially allowing more noise frames to propagate, which corresponds to a slight performance decrease. Based on these observations, θ is set to 0.75 in our experiments.

UPR Top- k Selection. Fig. 6 (b) analyzes the impact of top- k selection on model performance. The model achieves comparable results with $k = 8$ and 16, while $k = 4$ leads to a 1.36% accuracy drop and increased variance. A smaller k restricts the model to a limited subset of memory entries, potentially causing biased feature aggregation and unstable performance. Based on these observations, top- k is set to 8 in our experiments.

4 Conclusion

In this paper, we present a novel dual-pathway framework DSTED for surgical workflow recognition that effectively addresses two critical challenges: temporal instability and ambiguous phase recognition. By decoupling the objectives of temporal stabilization and discriminative enhancement, we introduce reliable memory propagation and uncertainty-aware prototype retrieval as distinct yet complementary mechanisms. RMP ensures temporal coherence by selectively propagating reliable historical features, while UPR enhances discriminative power by refining the representation of ambiguous frames through uncertainty-aware prototypes. Experimental results demonstrate that the proposed DSTED framework outperforms existing state-of-the-art methods, achieving significant improvements in both accuracy and temporal stability on the AutoLaparo dataset. Ablation studies confirm the contributions of each component, with further gains realized through the confidence-driven integration mechanism. The proposed approach highlights the importance of targeted and uncertainty-driven refinement for robust phase recognition, offering a promising direction for context-aware assistance in complex surgical procedures.

5 Acknowledges

This work described in this paper was supported by a grant from the ANR/RGC Joint Research Scheme sponsored by the Research Grants Council of the Hong Kong Special Administrative Region, China and the French National Research Agency (Project No. A-CUHK402/23)

References

- [1] Demir, K.C., Schieber, H., Weise, T., Roth, D., May, M., Maier, A., Yang, S.H.: Deep learning in surgical workflow analysis: a review of phase and step recognition. *IEEE J. Biomed. Health Inform.* **27**(11), 5405–5417 (2023)
- [2] Padoy, N., Blum, T., Ahmadi, S.-A., Feussner, H., Berger, M.-O., Navab, N.: Statistical modeling and recognition of surgical workflow. *Med. Image Anal.* **16**(3), 632–641 (2012)
- [3] Cao, J., Yip, H.-C., Chen, Y., Scheppach, M., Luo, X., *et al.*: Intelligent surgical workflow recognition for endoscopic submucosal dissection with real-time animal study. *Nature Commun.* **14**(1), 6676 (2023)
- [4] Yi, F., Jiang, T.: Hard frame detection and online mapping for surgical phase recognition. In: *Med. Image Comput. Comput.-Assist. Interv.*, pp. 449–457. Springer, Shenzhen, China (2019)
- [5] Jin, Y., Dou, Q., Chen, H., Yu, L., *et al.*: Sv-rcnet: workflow recognition from surgical videos using recurrent convolutional network. *IEEE Trans. Med. Imaging* **37**(5), 1114–1126 (2017)
- [6] Czempiel, T., Paschali, M., Keicher, M., Simson, W., *et al.*: Tecno: Surgical phase recognition with multi-stage temporal convolutional networks. In: *Med. Image Comput. Comput.-Assist. Interv.*, pp. 343–352 (2020)
- [7] Wang, L., Huang, B., Zhao, Z., Tong, Z., He, Y., Wang, Y., Wang, Y., Qiao, Y.: Videomae v2: Scaling video masked autoencoders with dual masking. In: *Proc. IEEE/CVF Conf. Comput. Vis. Pattern Recognit.*, pp. 14549–14560 (2023)
- [8] Wu, H., Wang, T.-H., Lechner, M., Hasani, R., Eckhoff, J.A., *et al.*: Holistic surgical phase recognition with hierarchical input dependent state space models. *arXiv preprint arXiv:2506.21330* (2025)
- [9] Wang, Z., Lu, B., Long, Y., Zhong, F., Cheung, T.-H., Dou, Q., Liu, Y.: Autolaparo: A new dataset of integrated multi-tasks for image-guided surgical automation in laparoscopic hysterectomy. In: *Med. Image Comput. Comput.-Assist. Interv.*, pp. 486–496 (2022)
- [10] He, K., Zhang, X., Ren, S., Sun, J.: Deep residual learning for image recognition.

In: Proc. IEEE Conf. Comput. Vis. Pattern Recognit., pp. 770–778 (2016)

[11] Jin, Y., Long, Y., Chen, C., Zhao, Z., Dou, Q., Heng, P.-A.: Temporal memory relation network for workflow recognition from surgical video. *IEEE Transactions on Medical Imaging* **40**(7), 1911–1923 (2021)